Electronic structures and optical properties of $(Ph_4P)MX_2$ (M = Cu, Ag; X = Cl, Br)

Dilruba A. Popy, ¹ Tielyr D. Creason, ¹ Zheng Zhang, ¹ David J. Singh, ² Bayram Saparov ^{1*} ¹ Department of Chemistry & Biochemistry, University of Oklahoma, Norman, OK 73019, USA ² Department of Physics and Astronomy, University of Missouri, Columbia, MO 65211, USA *Author to whom correspondence should be addressed: saparov@ou.edu

ORCID ID: Dilruba A. Popy: 0000-0001-5017-3274; Tielyr D. Creason: 0000-0003-1688-8115; Zheng Zhang: 0000-0003-2704-0355; David J. Singh: 0000-0001-7750-1485; Bayram Saparov: 0000-0003-0190-9585.

Abstract: In recent years, all inorganic copper(I) halides have emerged as an exciting new class of optical materials that demonstrate high-efficiency photoluminescence (PL) properties. Here, we report the synthesis and characterization of a series of hybrid copper(I) and silver halides (Ph₄P)MX₂ (M = Cu, Ag; X = Cl, Br) containing tetraphenylphosphonium (Ph₄P⁺) cation as the organic component. Addressing one of the shortcomings of all-inorganic copper(I) halides, inclusion of the bulky organic Ph₄P⁺ cation improves the stability of the hybrid compounds; (Ph₄P)MX₂ show no sign of degradation upon long-term ambient air exposure. The compounds are found to exhibit unusually weak light emission properties for Cu(I) and Ag(I) halides. Our combined experimental and density-functional theory (DFT) studies attribute the contrasting optical properties of these compounds to their unique crystal and electronic structures. This work provides new materials design perspectives to explore low cost and low toxicity metal halides for light emission applications.

Keywords:

Zero-dimensional hybrids, copper(I) halides, silver(I) halides, crystal growth, photoluminescence, structure-property relationships

1. Introduction

In recent years, the development of low-dimensional metal halides (LDMHs) has attracted significant attention owing to the low cost and low temperature solution processability as well as unique optical properties of LDMHs. The presence of highly localized charges and quantum confinement effects observed in LDMHs facilitate the formation of room-temperature stable excitons, recombination of which provides high-efficiency photoluminescence (PL) emission. The highest degree of charge localization is often observed in LDMHs with one-dimensional (1D) chain and zero-dimensional (0D) cluster structures, which can demonstrate self-trapped excitonic (STE) emission with up to unity Photoluminescence Quantum Yield (PLOY) [1-4]. In addition to their outstanding light emission efficiencies, LDMHs also demonstrate highly tunable crystal structures and chemical compositions – virtually endless combinations of all-inorganic and hybrid organic-inorganic metal halides maybe used in the construction of LDMHs. Historically, various lead halide families have been explored first due to their obvious connection with the parent lead halide perovskites used in photovoltaics (PV) [5-8]. However, their poor air and moisture stabilities along with the concerns relating to the toxicity of lead has motivated a global search for alternative lead-free metal halide families [9]. Consequently, many new families of lead-free emissive metal halide systems have been discovered in which Cd, Sn, In, Sb, Bi etc. have been used as a replacement for the toxic lead [10-14].

The recent discovery of copper(I) halide-based lighting materials such as Cs₃Cu₂X₅, K₂CuX₃ and CsCu₂X₃ (X = Cl, Br, I) families has been a significant development in this area [15-17]. Thus, all-inorganic copper(I) halides demonstrate PL emission efficiency up to 100% at room temperature and have low material cost and low toxicity compared to the lead-halide counterparts. However, poor stability of these materials (e.g., due to the oxidation of Cu⁺ to Cu²⁺ in ambient air) remains a concern that needs to be suitably addressed. In addition, light emission demonstrated by these Cu(I) halides is insensitive to various halogen or alkali metal substitutions due to the predominant contribution of Cu-3d and Cu-4s orbitals to the valence band maxima (VBM) and conduction band minima (CBM), respectively [16-18]. Interestingly, replacing copper with silver yields much improved stability of the materials such as Rb₂AgX₃, (NH₄)₂AgX₃ (X= Cl, Br, I), etc. [19, 20] In addition, the light emission in Ag(I) halides are more sensitive to the chemical substitutions on the alkali metal and halogen sites. On the other hand, the PL emission efficiency of Ag(I) halides is typically much lower than the corresponding copper(I) halides.

Yet another possible strategy to control the PL properties and improve stability of Cu(I) halide light emitters is to replace the alkali metal cations with an organic cation such as in the cases of (MA)₄Cu₂Br₆ (MA = methylammonium) [21], (TBA)CuBr₂ (TBA = tetrabutylammonium) [22], (TPA)CuCl₂ (TPA = tetrapropylammonium) [23], (TPA)CuI₂ [24], (Gua)₃Cu₂I₅ (Gua = guanidinium) [25], etc. The presence of bulky hydrophobic organic cations may improve the stability of the hybrid materials by preventing the oxidation of Cu⁺. Unlike the all-inorganic Cu(I) halides, which are typically blue emitters, the newly discovered organic-inorganic Cu(I) halides often show more red-shifted STE emission. It is hypothesized that the inclusion of structurally diverse organic cations in Cu(I) halides may also indirectly impact the observed PL properties since the coordination behavior of metals can be influenced by the choice of the organic molecules used in the construction of hybrids. For example, prior reports show that copper halides favor the formation of edge-sharing tetrahedral [Cu₂Br₆]⁴⁻ units in MA₄Cu₂Br₆, whereas linear [CuBr₂] units are formed in (TBA)CuBr₂ when bulky tetrabutylammonium (TBA) cations are used [21, 22]. In

these cases, metal halide units act as optically active centers and high photoluminescence efficiency is attributed to the electronic transition localized on the inorganic structural units. However, in principle, yet another way to control the PL emission profiles of Cu(I) halides is through the incorporation of photoactive organic molecules. To date, in-depth studies of the contribution of photoactive organic molecules in the photophysical properties of the hybrid Cu(I) and Ag(I) halides has not been conducted.

All-inorganic Cu(I) halides such as Cs₃Cu₂X₅ and K₂CuX₃ were all prepared and structurally characterized decades ago [26-28], however, their optoelectronic properties were not studied until recently [16, 29]. Similarly, there are still many other families of all-inorganic and hybrid copper(I) and silver(I) halides that have been reported since 19th century [28], and their optical properties are yet to be studied. The literature reported Cu(I) and Ag(I) halides show diverse structural building blocks unlike the high efficiency blue emitting all-inorganic copper(I) halides, which all have tetrahedral CuX₄ building blocks. To study the impact of the coordination environment of Cu(I) and Ag(I) on the optical properties of hybrid Cu(I)/Ag(I) halides, here, we report preparation, electronic structures and optical characterization of four 0D hybrid copper(I) and silver(I) halides (Ph₄P)CuCl₂ (1), (Ph₄P)CuBr₂ (2), (Ph₄P)AgCl₂ (3) and (Ph₄P)AgBr₂ (4), which were structurally characterized in several prior reports [30, 31]. Tetraphenylphosphonium (Ph₄P⁺) was chosen due to its ability to readily form crystalline hybrid organic-inorganic materials via a facile solution synthesis process, as well as the unique crystal structures it affords in (Ph₄P)MX₂ [10, 30-33]. We find that (Ph₄P)MX₂ demonstrate much improved air and thermal stability as compared to the allinorganic Cu(I) halides. Structural characterizations of these four compounds were performed using powder and single crystal X-ray diffraction measurements. Optical properties were studied via photoluminescence spectroscopy. For the first time, we also performed electrical measurements and X-ray response tests for single crystals of (Ph₄P)CuBr₂. Our experimental results on (Ph₄P)MX₂ are discussed in conjunction with the density-functional theory (DFT) calculation results to understand optical property and trends in this family.

2. Experimental Section

2.1. Materials: Copper(I) chloride (>99%, Sigma-Aldrich), copper(I) bromide (>99%, Alfa Aesar), silver chloride (99%, Alfa Aesar), silver bromide (99%, Alfa Aesar), tetraphenylphosphonium chloride (Ph4PCl) (98%, Sigma-Aldrich), tetraphenylphosphonium bromide (Ph4PBr) (>98%, TCI), N,N-dimethylformamide (DMF) (anhydrous, Sigma-Aldrich), and diethyl ether (>99.7%, Sigma-Aldrich) were purchased and used as received with no further purification. Reactions containing silver reagents were performed by wrapping the glass scintillation reaction vials with aluminum foil. All syntheses procedures were carried out in ambient air inside a fume hood unless otherwise stated.

2.2. $(Ph_4P)CuX_2$ (X = Cl, Br) synthesis

2.2.1. Single crystals via vapor-diffusion: A total of 0.5 g stoichiometric amounts of Ph₄PX and CuX were dissolved in 1 mL DMF (anhydrous) at room temperature to form a clear precursor solution. Inside a sealed container, 1.5 mL diethyl ether was diffused into the precursor solution overnight at room temperature. Vapor-diffusion produced ~0.6 cm long colorless block crystals,

which were washed with diethyl ether and dried at room temperature. The crystals were stored in a nitrogen-filled glovebox for further optical characterizations.

- 2.2.2. Single crystals via slow cooling of a saturated solution: A total of 2.0 g stoichiometric amounts of Ph₄PX and CuX were dissolved in 2 mL DMF (anhydrous) at 90 °C to form a clear precursor solution in a nitrogen filled glovebox. The precursor solution was then cooled to room temperature over the 72 hours period. Colorless block crystals of (Ph₄P)CuX₂ measuring up to 0.4 cm long were collected and stored under nitrogen atmosphere.
- 2.2.3. Single crystals via slow solvent evaporation: A total of 0.5 g stoichiometric amounts of Ph₄PX and CuX were dissolved in 1 mL DMF (anhydrous) at room temperature to form a clear precursor solution in a nitrogen-filled glovebox. The solvent was slowly evaporated at 40 °C over 72 hours period and 0.4 cm long colorless block crystals of (Ph₄P)CuX₂ were collected and stored under nitrogen atmosphere.

2.3. $(Ph_4P)AgX_2$ (X = Cl, Br) synthesis

- 2.3.1. Single crystals via vapor-diffusion: A total of 0.5 g stoichiometric amounts of Ph₄PX and AgX were dissolved in 3 mL DMF (anhydrous) at 80 °C to form a clear precursor solution. 1 cm long colorless block crystals were prepared by diffusing 1.5 mL diethyl ether into 1 mL precursor solution overnight at room temperature. Single crystals were washed with diethyl ether and dried at room temperature and pressure. Crystals were stored in a nitrogen-filled glovebox for further optical characterizations.
- 2.3.2. Single crystals via slow cooling of a saturated solution: A total of 2.0 g stoichiometric amounts of Ph₄PX and AgX were dissolved in 7 mL DMF (anhydrous) at 90 °C to form a clear precursor solution. The precursor solution was then cooled down to room temperature over the 72 hours period. 0.6 cm long colorless block crystals of (Ph₄P)AgX₂ were collected and stored under nitrogen atmosphere.
- 2.3.3. Single crystals via slow evaporation: A total of 0.5 g stoichiometric amounts of Ph₄PX and AgX were dissolved in 3 mL DMF (anhydrous) at 80 °C to form a clear precursor solution. Solvent was slowly evaporated at 50 °C over the 48 hours period and 0.8 cm long colorless block crystals of (Ph₄P)AgX₂ were collected and stored.

2.4. Powder X-ray Diffraction (PXRD) measurements

Powder X-ray diffraction (PXRD) measurements were carried out at room temperature for polycrystalline samples using a Rigaku MiniFlex600 system equipped with a Ni-filtered Cu K α radiation source. PXRD scans were performed in the 3 – 90° (2 θ) range with a step of 0.02°, and the XRD patterns were analyzed using a PDXL2 software package. Obtained PXRD patterns were fitted using the decomposition method. To test the air-stability of (Ph₄P)MX₂, powder samples were left on a laboratory bench under ambient air conditions (20 °C and 30% relative humidity) for four months during which periodic PXRD measurements were performed.

2.5. Single Crystal X-ray Diffraction (SCXRD) measurements

Single crystal X-ray diffraction (SCXRD) measurements were performed using a Bruker D8 Quest Kappa-geometry diffractometer with an Incoatec Ius microfocus Mo $K\alpha$ X-ray source and

a Photon II area detector. The data were corrected for absorption using the semiempirical method based on equivalent reflections, and crystal structures were solved by intrinsic phasing methods as embedded in the APEX3 v2015.5-2 program. Site occupancy factors were checked by freeing occupancies of each unique crystallographic positions. Details of the data collection and crystallographic parameters are given in Tables S1-S2. Atomic coordinates, equivalent isotropic displacement parameters, and selected interatomic distances, and bond angles are provided in Tables S3-S7. The Crystallographic Information Files (CIFs) were deposited in the Cambridge Crystallographic Data Centre (CCDC) database (deposition numbers 2176465-2176468).

2.6. Thermogravimetric Analysis and Differential Scanning Calorimetry (TGA/DSC) measurements

Simultaneous thermogravimetric analysis and differential scanning calorimetry (TGA/DSC) were measured on ~10 mg single crystal samples of the respective title compounds on a TA Instruments SDT 650 thermal analyzer system. Crystals were heated up from 25 °C to 475 °C under an inert nitrogen gas flow at a rate of 100 mL/min, with a heating rate of 5 °C/min.

2.7. Photoluminescence measurements

Room-temperature photoluminescence (PL) emission and PL excitation (PLE) measurements were carried out on single crystal samples of the respective title compounds using HORIBA Jobin Yvon Fluorolog-3 spectrofluorometer with Xenon lamp source and Quanta-Φ integrating sphere. Data were collected using the two-curve method in a varied range from 250 to 750 nm.

2.8. Diffuse reflectance measurements

UV-vis diffuse reflectance data were collected on powder samples of the title compounds using a PerkinElmer Lambda 750 UV-vis-NIR spectrometer with a 100 mm Spectralon InGaAs Integrating Sphere over a range of 250-1100 nm. Diffuse reflectance data were then transformed to pseudo-absorption spectra utilizing the Kubelka-Munk function $F(R) = \frac{\alpha}{S} = \frac{(1-R)^2}{2R}$, where α is the absorption coefficient, S is the scattering coefficient, and R is the reflectance.

2.9. Density Functional Theory (DFT) Calculations

Density functional theory (DFT) calculations were done for the four compounds using the generalized gradient approximation (GGA) of Perdew, Burke and Ernzerhof (PBE) [34]. These calculations were done using the general potential linearized augmented planewave (LAPW) method [35], as implemented in the WIEN2k code [36]. We used the augmented planewave plus local orbital augmentation for the H and C atoms [37], and the standard LAPW augmentation for the other atoms. We used LAPW sphere radii of 2.2 Bohr for Ag, Br, Cl and P, 1.95 Bohr for Cu, 1.03 Bohr for C and 1.0 Bohr for H, with the exception that we used 1.95 Bohr for Cl in (Ph4P)CuCl₂. The lattice parameters and space group symmetries were as obtained from experiment. However, we relaxed the internal coordinates of the atoms using total energy minimization with the PBE functional. This was necessary in particular to obtain the H positions, which could not be obtained reliably from the XRD. The optical properties were calculated using the optical package of WIEN2k.

2.10. Electrical measurements and X-ray response tests

A simple (Ph₄P)CuBr₂-based single crystal device for electrical measurements and X-ray response test was fabricated by brushing a high-quality silver paste (purchased from Ted Pella, Inc.) onto the two opposite sides of a single crystal. Current-voltage (I-V) and space-charge-limited-current (SCLC) measurements were performed using a Keithley 6487 pico-ammeter. Both the I-V and SCLC measurements were performed using a step of 5 V for voltage scan. For X-ray response test, the fabricated prototype single crystal-based detector was exposed to 8 keV soft X-rays, which are produced from a Rigaku MicroMax 007HF microfocus X-ray generator that is equipped with a Cu target. X-ray radiation dose rate was carefully calibrated using a commercial dosimeter.

3. Results and Discussion

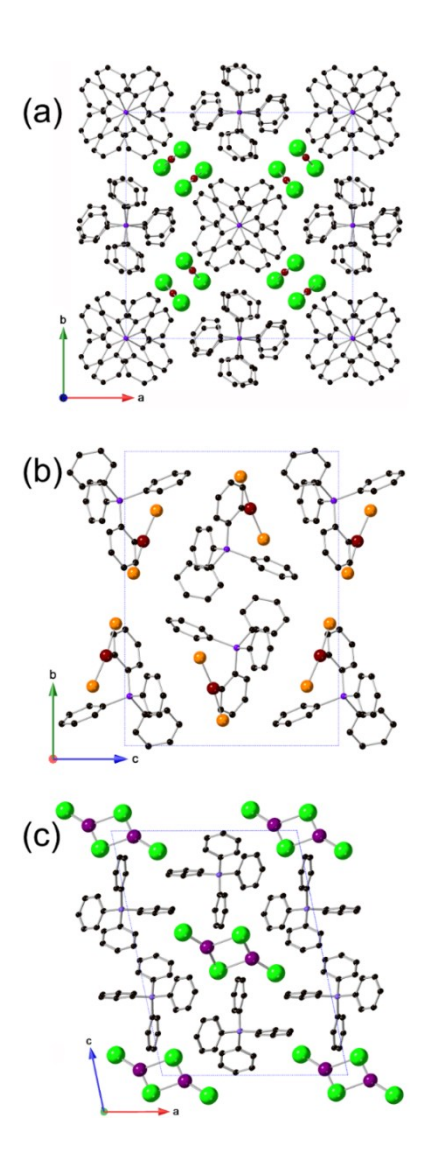


Fig. 1. Crystal structures of (a) (Ph₄P)CuCl₂, (b) (Ph₄P)CuBr₂, and (c) (Ph₄P)AgX₂ (X = Cl, Br). Brown, violet, green, orange, purple, and black spheres represent copper, silver, chloride, bromide, phosphorus, and carbon, respectively.

(Ph4P)CuCl₂ (1), (Ph4P)CuBr₂ (2), (Ph4P)AgCl₂ (3) and (Ph4P)AgBr₂ (4) single crystals of up to 1 cm long can be grown by three distinct solution synthesis methods including vapor-diffusion, solvent evaporation and slow cooling of saturated solutions. The detailed synthesis methods are described in the experimental section. The purity of products obtained from three different synthesis methods were ensured by PXRD measurements. Best quality crystals were obtained from the anti-solvent vapor diffusion method using DMF – diethyl ether solvents system and all optical characterizations were carried out using these crystals. The anti-solvent vapor diffusion method is also advantageous over the other two methods to synthesize these four compounds because it affords high quality crystals in the shortest time (see section 2.2 and 2.3). The crystals are colorless under ambient light (Fig. S1). The results of SCXRD experiments at 296 K for these four compounds are summarized in Table S1-S7 and crystal structures are shown in Fig. 1. The obtained crystal structure data are consistent with the prior reports [30, 31]. (Ph₄P)CuCl₂ crystallizes in the tetragonal crystal system in the non-centrosymmetric space group I-4, whereas (Ph₄P)CuBr₂ crystallizes in the monoclinic crystal system in the centrosymmetric space group $P2_1/c$. (Ph₄P)AgCl₂ and (Ph₄P)AgBr₂ are isostructural and crystallize in the monoclinic crystal system within the centrosymmetric space group $P2_1/n$.

Notably, the crystal structures of 1-4 significantly differ from that of the high-efficiency light emitting Cu(I) and Ag(I) halides, which are built upon tetrahedral MX4 units, e.g., Rb2CuX3, K_2CuX_3 , $CsCu_2X_3$, Rb_2AgX_3 , $(NH_4)_2AgX_3$ (X = Cl, Br), etc. [16-20]. In the 0D structures of 1 and **2.** Cu^+ is coordinated with two X leading to the formation of approximately linear $[CuX_2]$ units. The Cl-Cu-Cl bond angle is 175.59(6) while Br-Cu-Br bond angle is 173.39(3), suggesting the better linearity in [CuCl₂] unit compared to [CuBr₂] unit (Fig. S2). This is also in agreement with the bond lengths of Cu-Cl [2.0792(2) Å, 2.0807(2) Å] and Cu-Br [2.2190(2) Å, 2.2046(6) Å] in 1 and 2. In comparison, two Ag⁺ are coordinated with four X⁻ to form edge sharing approximate trigonal planar [Ag₂X₄]²- units in 3 and 4. The terminal Ag-X bond lengths are shorter than the bridging bond lengths. Two bridging X have different Ag-X bond lengths resulting slightly distorted dimeric [Ag₂X₄]²- units. [Ag₂Br₄]²- has less distortion compared to [Ag₂Cl₄]²- units. The intramolecular Ag--Ag distances are 3.665 Å in [Ag₂Cl₄]²⁻ and 3.582 Å in [Ag₂Br₄]²⁻ (Fig. S2), which is higher than the sum of van der Waals radii of two Ag atoms (3.40 Å), eliminating the possibility of the existence of Ag-Ag bond [38]. The metal halide units of these four compounds are completely isolated from the other nearest metal halide units in the corresponding crystal lattices and embedded in an inert matrix of bulky Ph₄P⁺ cations; this allows the formation of true 0D structures with well-separated metal halide anions. Moreover, the organic units invariably stack in two different parallel columns maintaining P--P distances ranging from 7.278 Å to 7.463 Å, and inorganic units occupy the holes between the columns. Interestingly, in compound 1, phenyl rings stack in eclipsed position in one column along c-axis while the other column consists of staggered phenyl rings. In all other three compounds, phenyl rings do not possess such type of arrangement. Significantly, the distances of Cu--Cu and Ag--Ag of nearest neighbors in compounds 1 to 4 are 7.622 Å, 7.119 Å, 8.024 Å and 7.66 Å, respectively. These large distances of nearest neighbors illustrate an almost negligible interactions between the adjacent anion clusters. The shortest intermolecular aromatic C--C distances of 3.330 Å, 3.696 Å, 3.459 Å and 3.875 Å in compounds 1 to 4, respectively, suggest the presence of π -stacking interactions [39]. These strong π -stacking interactions between the organic layers contributes to stabilizing the structure. Consequently, the compact packing of Ph₄P⁺ phenyl rings and smaller metal halide units provide the rigidity to the crystal structures of these compounds.

The unusual presence of linear and trigonal planar coordination environments in **1-4**, e.g., as compared to the all-inorganic tetrahedral copper(I) halide light emitters [16, 17], can be related to the templating nature of the organic cation used in this study. Thus, the delocalized charge density of Ph₄P⁺ and its larger size hinders the formability of tetrahedral coordination around copper (i.e., [CuX₄]³⁻), and instead, leads to the formation of discrete linear [CuX₂]⁻ units in **1** and **2** [30]. Similarly, silver halides form trigonal planar units in **3** and **4** [31]. These results support the conjecture that large cations with highly delocalized positive charge promote the formation of smaller, low charge metal halide units [28]. Note that this structure rationalization can also be tied to Pauling's rules – the lower charges on the anionic metal halide units separated by larger Ph₄P⁺ cations yields more stable structures (i.e., locally electroneutral) as an opposed to [MX₄]³⁻ tetrahedra separated by Ph₄P⁺ [40].

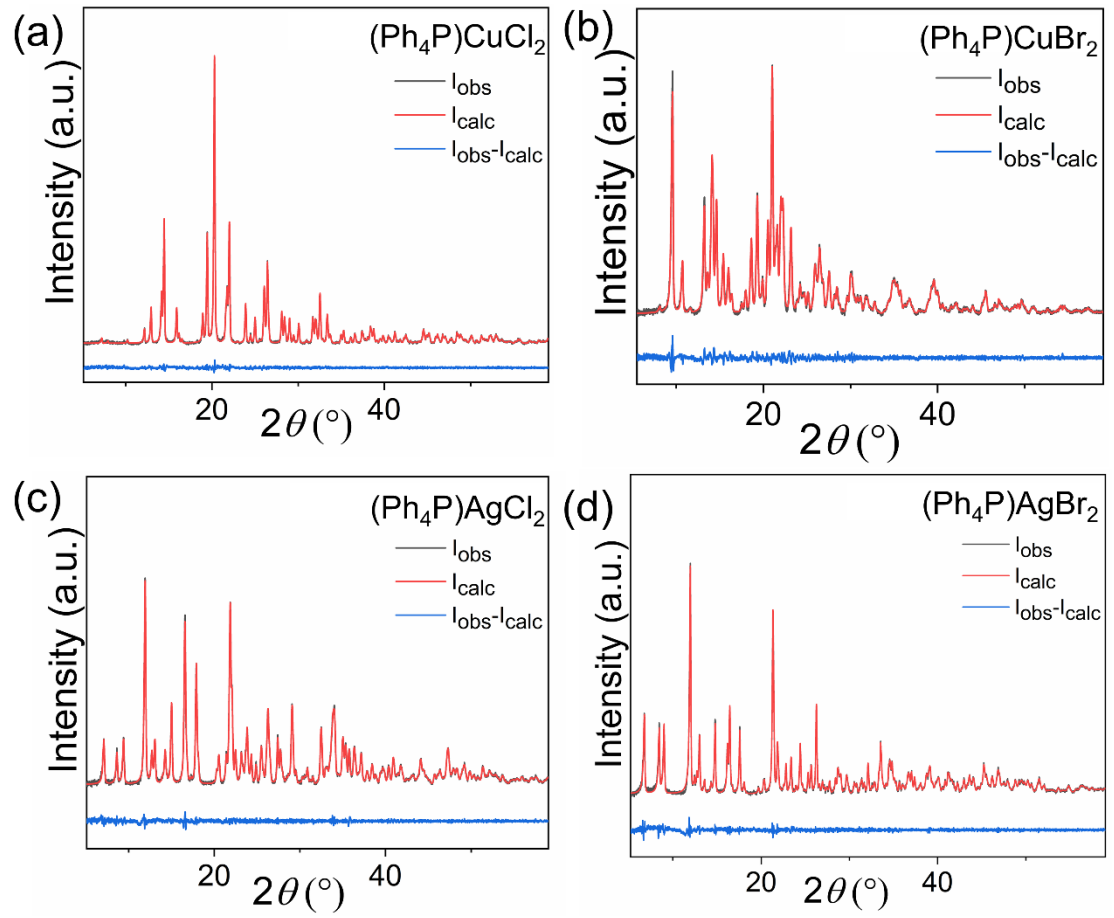


Fig. 2. Room-temperature PXRD patterns (in black) fitted using the Pawley method (in red) for (a) (Ph₄P)CuCl₂, (b) (Ph₄P)CuBr₂, (c) (Ph₄P)AgCl₂, and (d) (Ph₄P)AgBr₂. Difference between the measured and calculated patterns are shown in blue.

Our room-temperature powder X-ray diffraction (PXRD) data for 1-4 confirmed the high crystallinity and phase purity of the products obtained from the solution synthesis methods used in this work (Fig. 2). To determine the ambient air stability of the as-grown crystals, periodic PXRD measurements were carried out over a 4-month period under room temperature and ambient air conditions (Fig. S3). None of the samples showed degradation or decomposition. As a comparison, all-inorganic Cu(I) halide light emitters suffer from poor air stability due to

hygroscopicity and/or oxidation of Cu(I) [16-18]. Here, the large organic cation Ph₄P⁺ likely acts as a protective barrier for the inorganic molecular anions, preventing their degradation. Moreover, thermogravimetric analysis (TGA) measurements suggest the improved thermal stability of this series with no significant weight loss up to ~400 °C (Fig. S4). These results suggest considerable improvements of both long-term air stability and thermal stability of **1-4** compared to other reported all-inorganic and hybrid organic-inorganic copper and silver halides, such as Rb₂CuX₃, K₂CuX₃, [Me-Py]CuI₂, [(Me)₂-DABCO]Cu₂I₄, [Me-MePy]Cu₂I₃, [H₂DABCO]Cu₃X₅, Rb₂AgX₃, (NH₄)₂AgX₃ (X= Cl, Br, I), etc. [16-20, 41]. The differential scanning calorimetry (DSC) results demonstrate that compounds **1** to **4** show a phase change at 208.13 °C, 209.16 °C, 211.51 °C and 220.22 °C, respectively, which correspond to the melting transitions of the compounds.

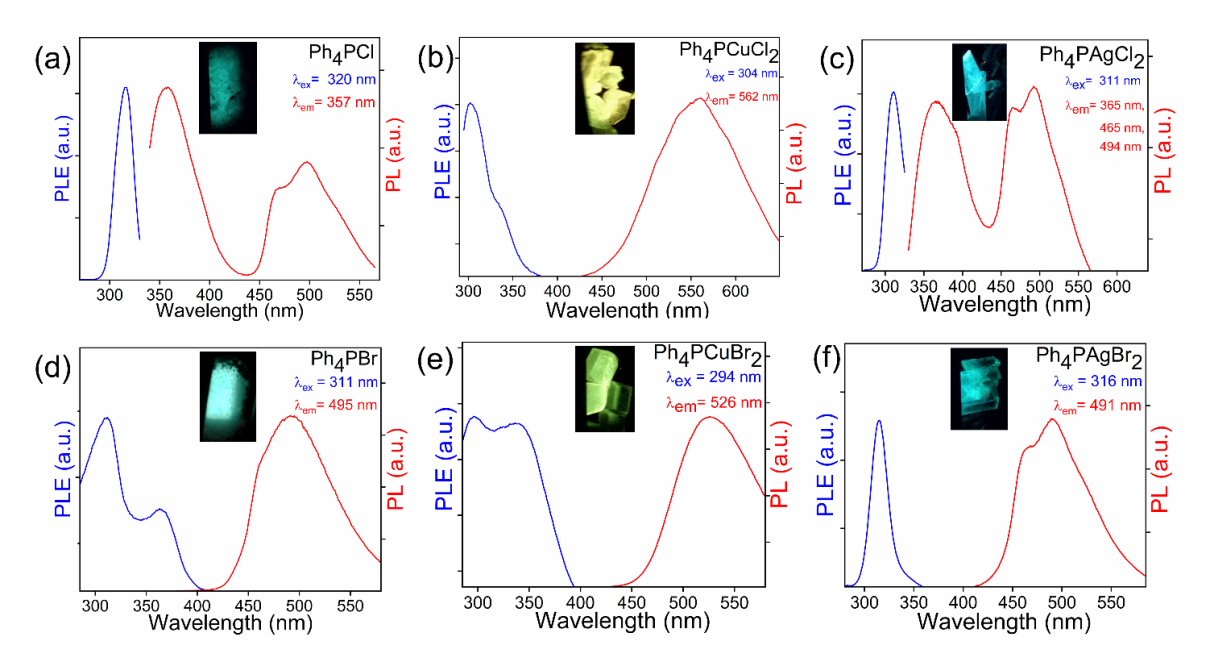


Fig. 3. Photoluminescence excitation (PLE) (blue) and photoluminescence emission (PL) (red) spectra at room temperature: (a) Ph₄PCl, (b) (Ph₄P)CuCl₂, (c) (Ph₄P)AgCl₂, (d) Ph₄PBr, (e) (Ph₄P)CuBr₂, and (f) (Ph₄P)AgBr₂. The insets show the light emission of the corresponding compound under UV radiation.

To understand the relationship between the unique structures of **1-4** and their photophysical properties, room-temperature UV-vis optical absorption and PL measurements were performed. Photoluminescence excitation (PLE) and emission (PL) spectra of Ph₄PX, (Ph₄P)CuX₂ and (Ph₄P)AgX₂ (X = Cl and Br) are shown in Fig. 3. Our PL/PLE spectra for Ph₄P halides are consistent with the previously reported spectra [42]. Immediately noticeable is the fact that the bluish green color of light emission and PL/PLE spectra of **3** and **4** are similar to that for the corresponding organic precursor salts Ph₄PX. Single crystals of compound **3** show three distinguishable emission peaks at 365 nm, 465 nm, and 494 nm for the excitation wavelength at 311 nm. Single crystals of **4** have emission peak at 491 nm for the excitation wavelength of 311 nm. The nature of these PL spectra is suggestive as the organic dominated PL emission for both

hybrid silver halides. However, unlike the silver halides, both Ph₄P copper(I) halides 1 and 2 show a red shifted and broadband PL emission peaks compared to the precursor organic salts, which can be attributed to the contribution of copper in these electronic transitions; Cu(I) centered transitions were also observed in other copper(I) halide luminescent materials [16, 17, 21-24]. Single crystals of compounds 1 and 2 emit yellow and greenish yellow light with PL emission maxima at 562 nm and 526 nm for PL excitation at 304 nm and 294 nm, yielding Stokes shifts values of 258 nm and 232 nm, respectively. These types of large Stokes shifts and broadband emission of copper(I) halides are normally attributed to midgap emissions originating from radiative recombination of either STEs or defect-bound excitons (DBEs) [21, 22, 43-45]. However, in the present case, the involvement of both organic and inorganic components in the PL spectra may be indicative of the presence of charge transfer excitons (see below) [46].

To better understand the mechanisms of optical transitions in these materials, diffuse reflectance measurements were conducted on polycrystalline powder samples of 1-4 to determine their optical absorption properties (Fig. 4). The measurements suggest strong onsets of absorption near 4 eV for all the compounds. However, a recent study on 2 by Xu et.al. [43] reports a much lower band gap of 2.57 eV. Therefore, we also conducted a close inspection of the lower energy region, which revealed that all four compounds have very weak absorption humps near 2.6 eV (insets in Fig. 4). Absorption in this lower energy region is so weak, such that the crystals look colorless in visible light (Fig. S1). Note that the experimental optical absorption spectra have been reproduced and explained by our DFT computational work (Fig. S5). The strong onsets of absorption at ~4 eV is assigned to the electronic transitions on the inorganic structural units, while the weak absorption features at ~ 2.6 eV can be attributed to the transitions from the inorganic to organic units. Interestingly, Peng et. al. also reported the strong absorption near 4 eV for [CuX₂] units which supports our assignment of electronic transitions in inorganic units for compounds 1 and 2 [22, 23, 47]. Importantly, the lower energy region absorption features for 1-4 may contribute to the self-absorption of the emitted light, which can reduce the emission efficiency of these compounds.

The estimated photoluminescence quantum yield (PLQY) values were measured to be nearly 1% for these four materials. The quenched PL in 1-4 (e.g., as opposed to ~100% PLQY demonstrated by K₂CuCl₃ [16]) can be explained using two approaches. First, in the high-efficiency light emitting Cu(I) halides, the photoexcitation causes the transient formation of Cu²⁺, and several groups have suggested that the formation of Cu²⁺ is followed by Jahn-Teller distortion of the structure, facilitating the formation of high stability STEs [29]. In the case of 1 and 2, the presence of linear [CuX₂]⁻ units would rule out this mechanism as a possibility since Jahn-Teller effect does not apply to the linear coordination environment. Another explanation more specific to 1-4, the electronic transitions (both absorption and emission) involve both organic and inorganic structural components in these compounds (see the DFT results below). The transitions between spatially separate structural parts leads to a very small optical matrix elements, which is in turn results in very low optical absorption coefficients in the lower energy region (Fig. S5). Important for PL, the spatial separation of excited electrons and holes result in very poor PL efficiencies. Note that the observations made for 1-4 in this work is also in agreement with a recent report on a

trigonal planar Cu^IX₃ unit-based PyCs₃Cu₂Br₆ (Py = pyridinium), which also shows quenched PL emission due to the spatial separation of electrons and holes in different structural segments [46].

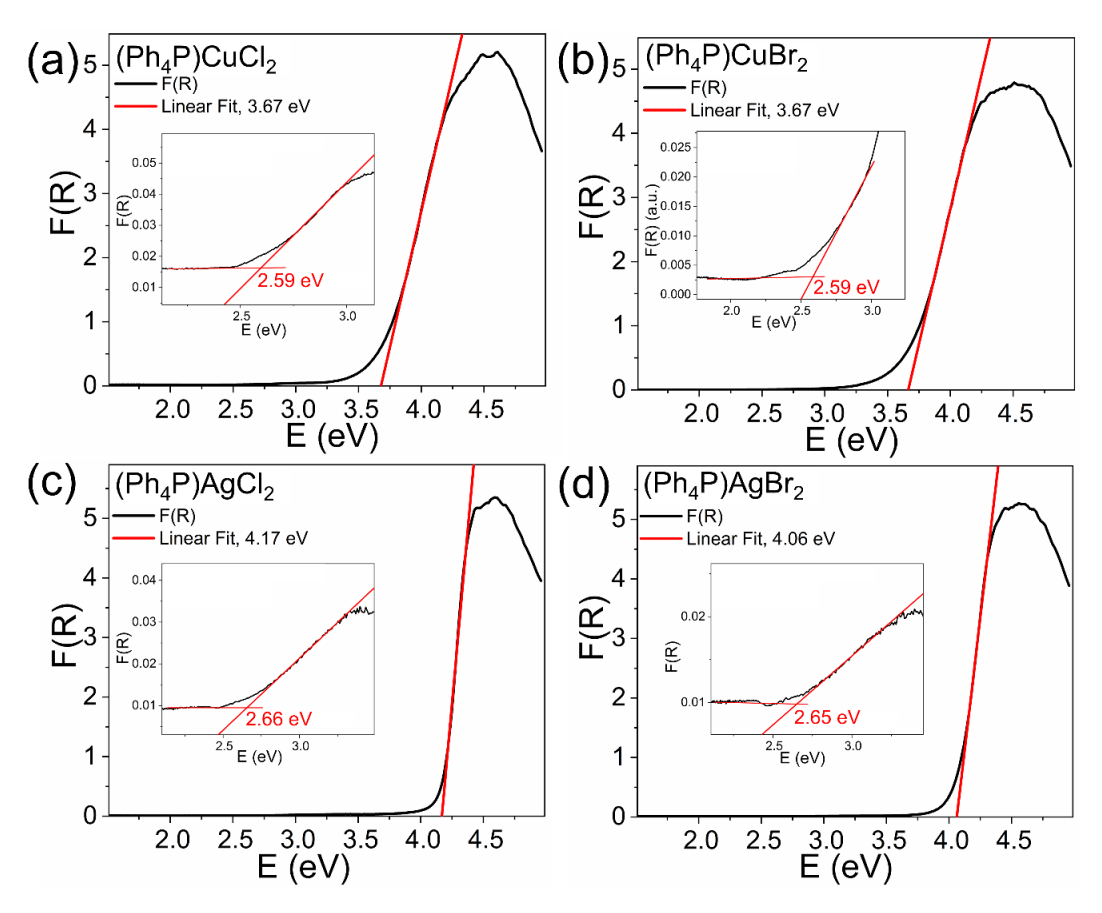


Fig. 4. Optical absorption data obtained using the Kubelka–Munk function, F(R), for (a) (Ph₄P)CuCl₂, (b) (Ph₄P)CuBr₂, (c) (Ph₄P)AgCl₂, and (d) (Ph₄P)AgBr₂. The insets show very weak lower energy absorption features that represent the true optical band gaps for **1-4**.

To better understand the optical properties of 1-4, DFT calculations with the general potential linearized planewave (LAPW) method were performed. For all these four compounds, the valence band maxima (VBM) are from antibonding metal d – halogen p combinations, with strong metal d character, whereas the conduction band minima (CBM) are predominantly from the organic states (Fig. 5). Although qualitatively similar, there are noticeable differences in the electronic structures of Cu(I) (i.e., 1 and 2) and Ag(I) halides (i.e., 3 and 4). Thus, the Ag compounds have broader, more hybridized metal d bands, therefore, the relative contribution of the Ag 4d orbitals to the VBM of 3 and 4 is less compared to the contribution of Cu 3d orbitals to the VBM of 1 and 2. As a result, the PL spectra of the compounds 3 and 4 are more similar to the PL spectra of Ph₄PX, where transition occurs from halogen atomic orbitals to the p orbitals of the organic units [48]. The electronic structures show states coming from the organic part of the structure from about 2 eV to close to 4 eV in the conduction band (CB). The optical matrix elements from the valence

band to these states is very small, resulting in a very weak onset of absorption in the calculated optical absorption spectra for 1-4 (Fig. S5). The large onset of the absorption spectra at ~4 eV in all compounds is attributed to the transitions localized on the inorganic units. Note that these computational results are in excellent agreement with our experimental optical absorption and PLE spectra (Fig. 3 and 4). The high energy photoexcitation of the inorganic structural units in (Ph4P)MX2 is followed by a quick relaxation of the excited electron to the lowest-lying excited state as per Kasha's rule [49], which in the case of 1-4 is mainly on the organic Ph4P⁺ molecules. The spatial separation of holes on the inorganic anions and electrons on the organic cations results in much lower emission efficiencies of 1-4 as compared to the highly luminescent Cu(I) and Ag(I) halides reported to date. This is unlike the case of organometallic Cu(I) halides that have direct Cu-to-organic bonding that allows close proximity of electron and hole localization, leading to efficient photoemission properties [50, 51].

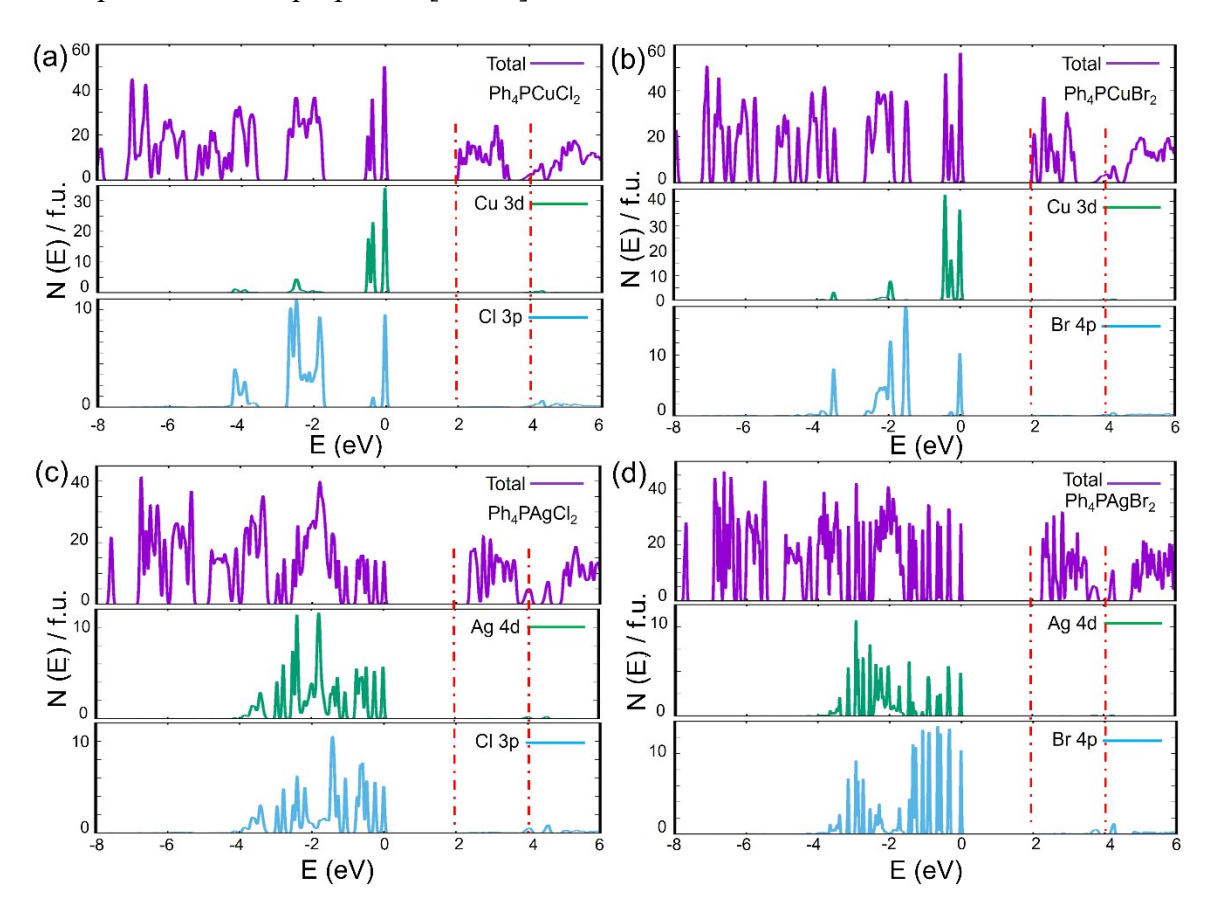


Fig. 5. Density of states plots for (a) (Ph₄P)CuCl₂, (b) (Ph₄P)CuBr₂, (c) (Ph₄P)AgCl₂, and (d) (Ph₄P)AgBr₂.

In addition to the fundamental studies of their unusual optical properties, copper(I) halides such as Rb₂CuBr₃ and Cs₃Cu₂I₅ have been attracting the interest of researchers due to their promising electrical and X-ray scintillation properties [52]. Although the poor light emission properties of **1-4** do not allow for their consideration for scintillator applications, we investigated the electronic semiconducting properties of **1-4**. An as-grown (Ph₄P)CuBr₂ single crystal (SC) with large surface

area was selected for electrical characterizations. Fig. 6a shows the photon absorption coefficient of 3 (covering the energy range from soft X-rays to high-energy gamma-rays) compared to that of several other typical X-ray detector materials, including cadmium telluride (CdTe), methylammonium lead bromide (MAPbBr₃) and cesium lead bromide (CsPbBr₃) perovskites (the photon attenuation data is available online through the XCOM photon cross section database). The photon attenuation ability of **3** is comparatively lower due to its low average atomic number (5.79). However, X-rays have relatively low penetration ability compared to high-energy gamma-rays, thus warranting the potential use of (Ph₄P)CuBr₂ for X-ray radiation detection. The resistivity of 3 SC was determined to be $4.79 \times 10^{12} \ \Omega$ ·cm from the I-V measurement as shown in the Fig. 6b, which is high enough for reducing the detector leakage current for performing sensitive X-ray radiation detection [53]. In addition, the defect trap levels, and charge carrier mobility of semiconductors plays an important role when developing semiconductor materials for ionizing radiation detection [54]. In this study, we adopted the space-charge-limited-current (SCLC) method [55] that has been widely used for studying metal halide perovskites (MHPs) to investigate the defect trap level of the as-grown (Ph₄P)CuBr₂ SC (see Fig. 6c). The estimated density of trap states (n_t) is 6.11×10⁹ cm⁻³, which is comparable to several other metal halides MAPbI₃ 9.6×10⁹ cm⁻³ [56], Cs₃Bi₂I₉ 1.4×10¹⁰ cm⁻³ [57], and Rb₄Ag₂BiBr₉ 3.33×10¹⁰ cm⁻³ [58].

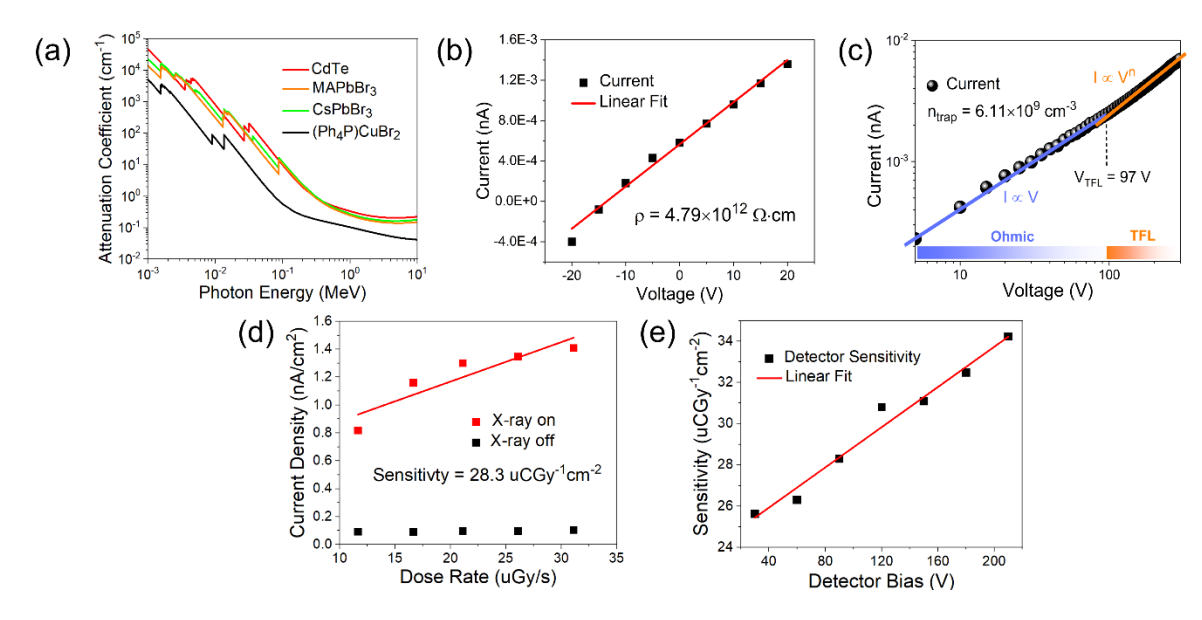


Fig. 6. (a) Plot of the photon attenuation coefficient vs. photon energy (from 1 keV to 10 MeV, covering the energy range from soft X-rays to high-energy gamma-rays) for CdTe, MAPbBr₃, CsPbBr₃ perovskites, and (Ph₄P)CuBr₂. (b) Current-voltage (I-V) measurement results used to determine the semiconductor resistivity of a (Ph₄P)CuBr₂ single crystal. (c) Measured space-charge-limited-current (SCLC) curve for (Ph₄P)CuBr₂. (d) X-ray radiation response measurement results using a (Ph₄P)CuBr₂ single crystal to determine the detector sensitivity. (e) X-ray detector sensitivity measurement of a (Ph₄P)CuBr₂ single crystal with the applied detector voltage bias.

To investigate the potential use of the (Ph₄P)CuBr₂ SCs for semiconducting radiation detection, we fabricated a prototype X-ray radiation detector. The fabricated X-ray detector performance was

evaluated by exposing (Ph₄P)CuBr₂ SC to 8 keV soft X-ray radiation. The fabricated detector showed significant response to soft X-rays when the X-ray beam was turned on (see Fig. 6d). Moreover, the detector sensitivity, which is an important figure of merit for evaluating the X-ray detector performance, was determined to be 28.3 uCGy⁻¹cm⁻² (at an electric field of 36 V/mm). The detector sensitivity could be further enhanced to 34.23 uCGy⁻¹cm⁻², when the detector is biased at a higher voltage of 210 V with the corresponding electric field of 84 V/mm (Fig. 6e). It is noted that although the determined detector sensitivity here for (Ph₄P)CuBr₂ SCs is lower compared to several other metal halides, such as MAPbBr₃ (259.9 uCGy⁻¹cm⁻² at electric field of ~0.83 V/mm) [59] and Cs₂AgBiBr₆ (105 uCGy⁻¹cm⁻² at electric field of 25 V/mm) [60], few material optimization strategies including surface passivation and thermal annealing should be able to further enhance the detector performance based on this material.

4. Conclusion

In summary, this work reports preparation, structural, optical, and electrical characterizations of four hybrid metal halides (Ph₄P)MX₂ (where M = Cu, Ag; X = Cl, Br). These hybrid copper(I) and silver(I) halides exhibit 0D crystal structures containing fully isolated metal-halide units closely packed by bulky organic cations. Inclusion of the bulky organic cation Ph₄P⁺ results in much improved air and thermal stability of these materials. In contrast to the high-efficiency allinorganic Cu(I) and Ag(I) halide light emitters, the PL emission efficiencies of (Ph₄P)MX₂ are rather weak with the measured PLQY values of around 1%. The quenched PL emission in (Ph₄P)MX₂ is attributed to their unique crystal and electronic structures. Thus, the crystal structures of (Ph₄P)MX₂ are built upon linear [CuX₂]⁻ and dimeric [Ag₂X₄]²- units, both of which have large band gaps of around ~4 eV. The organic Ph₄P⁺ cations essentially form midgap states, which provide a route for spatial separation of excited electrons and holes, and quenched PL in (Ph₄P)MX₂. Therefore, for improved PL, the design of hybrid organic-inorganic Cu(I) and Ag(I) halides should involve type I alignment in which VBM and CBM are both localized either on the organic or inorganic component such as in the cases of the related (TBA)CuCl₂ and (TBA)CuBr₂, which have been reported to exhibit STEs in isolated photoactive [CuX₂] units [61]. Importantly, although the weak PL efficiency of (Ph₄P)MX₂ is a negative result, the quenched PL in nontetrahedral Cu(I) and Ag(I) halides is a significant result, as it shows the importance of the energy band alignment of organic and inorganic units in hybrid organic-inorganic halides. This study will help researchers to design new families of high-efficiency and high stability Cu(I) and Ag(I) halide light emitters.

CRediT authorship contribution statement

Dilruba A. Popy: Carried out experiments, analyzed results, wrote the manuscript. Tielyr D. Creason: Analyzed data, proofread the manuscript. Zheng Zhang: Carried out electrical measurements, X-ray response tests and wrote the corresponding part of the manuscript. David J. Sing: Performed computational studies and wrote the corresponding part of the manuscript. Bayram Saparov: Conceptualized the study, acquired funding, managed the project, and wrote and reviewed the manuscript.

Declaration of competing interest

The authors declare that they have no known competing financial interests or personal relationships that could have appeared to influence the work reported in this paper.

Acknowledgement

This work was supported by the National Science Foundation (NSF DMR-2045490). We thank Dr. Douglas Powel for the help with SCXRD measurements (supported by NSF grant CHE-1726630). X-ray response tests were conducted at the X-ray lab located at the Biomolecular Structure Core (BSC)-Norman, University of Oklahoma, which is supported in part by an Institutional Development Award (IDeA) from the National Institute of General Medical Sciences of the National Institutes of Health (Award P20GM103640), the National Science Foundation (Award 0922269), and the University of Oklahoma Department of Chemistry and Biochemistry. We thank Dr. Leonard Thomas for his assistance with the X-ray response measurements. Dr. Dhritiman Banerjee and Isaiah W. Gilley are acknowledged for their constructive discussions and help with data analysis.

Appendix A. Supplementary data

Supplementary data to this article can be found online at https://www.sciencedirect.com/journal/journal-of-solid-state-chemistry/

References

- [1] L. Zhou, J.-F. Liao, D.-B. Kuang, An Overview for Zero-Dimensional Broadband Emissive Metal-Halide Single Crystals, Adv. Opt. Mater. 9 (17) (2021) 2100544, https://doi.org/10.1002/adom.202100544
- [2] R. Roccanova, A. Yangui, H. Nhalil, H. Shi, M.-H. Du, B. Saparov, Near-Unity Photoluminescence Quantum Yield in Blue-Emitting $Cs_3Cu_2Br_{5-x}I_x$ ($0 \le x \le 5$), ACS Appl. Electron. Mater. 1 (3) (2019) 269-274, 10.1021/acsaelm.9b00015
- [3] D. Han, H. Shi, W. Ming, C. Zhou, B. Ma, B. Saparov, Y.-Z. Ma, S. Chen, M.-H. Du, Unraveling Luminescence Mechanisms in Zero-Dimensional Halide Perovskites, J. Mater. Chem. C 6 (24) (2018) 6398-6405, 10.1039/C8TC01291A
- [4] C. Zhou, H. Lin, Q. He, L. Xu, M. Worku, M. Chaaban, S. Lee, X. Shi, M.-H. Du, B. Ma, Low Dimensional Metal Halide Perovskites and Hybrids, Mater. Sci. Eng. R Rep. 137 (2019) 38-65, https://doi.org/10.1016/j.mser.2018.12.001
- [5] H. Yuan, F. Massuyeau, N. Gautier, A.B. Kama, E. Faulques, F. Chen, Q. Shen, L. Zhang, M. Paris, R. Gautier, Doped Lead Halide White Phosphors for Very High Efficiency and Ultra-High Color Rendering, Angew. Chem., Int. Ed. 59 (7) (2020) 2802-2807, https://doi.org/10.1002/anie.201910180
- [6] H. Lin, C. Zhou, M. Chaaban, L.-J. Xu, Y. Zhou, J. Neu, M. Worku, E. Berkwits, Q. He, S. Lee, X. Lin, T. Siegrist, M.-H. Du, B. Ma, Bulk Assembly of Zero-Dimensional Organic Lead Bromide Hybrid with Efficient Blue Emission, ACS Mater. Lett. 1 (6) (2019) 594-598, 10.1021/acsmaterialslett.9b00333
- [7] S.K. Ha, C.M. Mauck, W.A. Tisdale, Toward Stable Deep-Blue Luminescent Colloidal Lead Halide Perovskite Nanoplatelets: Systematic Photostability Investigation, Chem. Mater. 31 (7) (2019) 2486-2496, 10.1021/acs.chemmater.8b05310
- [8] A. Yangui, R. Roccanova, Y. Wu, M.-H. Du, B. Saparov, Highly Efficient Broad-Band Luminescence Involving Organic and Inorganic Molecules in a Zero-Dimensional Hybrid Lead Chloride, J. Phys. Chem. C 123 (36) (2019) 22470-22477, 10.1021/acs.jpcc.9b05509
- [9] L. Lanzetta, N. Aristidou, S.A. Haque, Stability of Lead and Tin Halide Perovskites: The Link between Defects and Degradation, J. Phys. Chem. Lett. 11 (2) (2020) 574-585, 10.1021/acs.jpclett.9b02191
- [10] S. Liu, X. Fang, B. Lu, D. Yan, Wide Range Zero-Thermal-quenching Ultralong Phosphorescence from Zero-Dimensional Metal Halide Hybrids, Nat. Commun. 11 (1) (2020) 4649, 10.1038/s41467-020-18482-w
- [11] C. Zhou, H. Lin, Y. Tian, Z. Yuan, R. Clark, B. Chen, L.J. van de Burgt, J.C. Wang, Y. Zhou, K. Hanson, Q.J. Meisner, J. Neu, T. Besara, T. Siegrist, E. Lambers, P. Djurovich, B. Ma, Luminescent Zero-Dimensional Organic Metal Halide Hybrids with Near-unity Quantum Efficiency, Chem. Sci. 9 (3) (2018) 586-593, 10.1039/C7SC04539E

- [12] L. Zhou, J.-F. Liao, Z.-G. Huang, J.-H. Wei, X.-D. Wang, W.-G. Li, H.-Y. Chen, D.-B. Kuang, C.-Y. Su, A Highly Red-Emissive Lead-Free Indium-Based Perovskite Single Crystal for Sensitive Water Detection, Angew. Chem., Int. Ed. 58 (16) (2019) 5277-5281, https://doi.org/10.1002/anie.201814564
- [13] H. Peng, Y. Tian, X. Wang, T. Huang, Y. Xiao, T. Dong, J. Hu, J. Wang, B. Zou, Bulk Assembly of a 0D Organic Antimony Chloride Hybrid with Highly Efficient Orange Dual Emission by Self-trapped States, J. Mater. Chem. C 9 (36) (2021) 12184-12190, 10.1039/D1TC02906A
- [14] K.M. McCall, C.C. Stoumpos, S.S. Kostina, M.G. Kanatzidis, B.W. Wessels, Strong Electron–Phonon Coupling and Self-Trapped Excitons in the Defect Halide Perovskites A₃M₂I₉ (A = Cs, Rb; M = Bi, Sb), Chem. Mater. 29 (9) (2017) 4129-4145, 10.1021/acs.chemmater.7b01184
- [15] J. Li, T. Inoshita, T. Ying, A. Ooishi, J. Kim, H. Hosono, A Highly Efficient and Stable Blue-Emitting Cs₅Cu₃Cl₆I₂ with a 1D Chain Structure, Adv. Mater. 32 (37) (2020) e2002945, 10.1002/adma.202002945
- [16] T.D. Creason, T.M. McWhorter, Z. Bell, M.-H. Du, B. Saparov, K₂CuX₃ (X = Cl, Br): All-Inorganic Lead-Free Blue Emitters with Near-Unity Photoluminescence Quantum Yield, Chem. Mater. 32 (14) (2020) 6197-6205, 10.1021/acs.chemmater.0c02098
- [17] R. Roccanova, A. Yangui, G. Seo, T.D. Creason, Y. Wu, D.Y. Kim, M.-H. Du, B. Saparov, Bright Luminescence from Nontoxic CsCu₂X₃ (X = Cl, Br, I), ACS Materials Letters 1 (4) (2019) 459-465, 10.1021/acsmaterialslett.9b00274
- [18] T.D. Creason, A. Yangui, R. Roccanova, A. Strom, M.-H. Du, B. Saparov, Rb₂CuX₃ (X = Cl, Br): 1D All-Inorganic Copper Halides with Ultrabright Blue Emission and Up-Conversion Photoluminescence, Adv. Opt. Mater. 8 (2) (2020) 1901338, https://doi.org/10.1002/adom.201901338
- [19] P. Kumar, T.D. Creason, H. Fattal, M. Sharma, M.-H. Du, B. Saparov, Composition-Dependent Photoluminescence Properties and Anti-Counterfeiting Applications of A_2AgX_3 (A = Rb, Cs; X = Cl, Br, I), Adv. Funct. Mater. 31 (48) (2021) 2104941, https://doi.org/10.1002/adfm.202104941
- [20] T.D. Creason, H. Fattal, I.W. Gilley, T.M. McWhorter, M.-H. Du, B. Saparov, (NH₄)₂AgX₃ (X = Br, I): 1D Silver Halides with Broadband White Light Emission and Improved Stability, ACS Mater. Au 1 (1) (2021) 62-68, 10.1021/acsmaterialsau.1c00009
- [21] H. Peng, S. Yao, Y. Guo, R. Zhi, X. Wang, F. Ge, Y. Tian, J. Wang, B. Zou, Highly Efficient Self-Trapped Exciton Emission of a (MA)₄Cu₂Br₆ Single Crystal, J. Phys. Chem. Lett. 11 (12) (2020) 4703-4710, 10.1021/acs.jpclett.0c01162
- [22] H. Peng, Y. Tian, Z. Zhang, X. Wang, T. Huang, T. Dong, Y. Xiao, J. Wang, B. Zou, Bulk Assembly of Zero-Dimensional Organic Copper Bromide Hybrid with Bright Self-Trapped

- Exciton Emission and High Antiwater Stability, J. Phys. Chem. C 125 (36) (2021) 20014-20021, 10.1021/acs.jpcc.1c05065
- [23] H. Peng, Y. Tian, X. Wang, T. Dong, Z. Yu, Y. Xiao, Z. Zhang, J. Wang, B. Zou, Highly Efficient Broadband Green Emission of (TPA)CuCl₂ Single Crystals: Understanding the Formation of Self-Trapped States, J. Phys. Chem. C 126 (19) (2022) 8545-8552, 10.1021/acs.jpcc.2c02114
- [24] L. Lian, S. Wang, H. Ding, G. Liang, Y.-B. Zhao, H. Song, X. Lan, J. Gao, R. Chen, D. Zhang, J. Zhang, Single-Component White-Light Emitters with Excellent Color Rendering Indexes and High Photoluminescence Quantum Efficiencies, Adv. Opt. Mater. 10 (1) (2022) 2101640, https://doi.org/10.1002/adom.202101640
- [25] H. Peng, X. Wang, Y. Tian, B. Zou, F. Yang, T. Huang, C. Peng, S. Yao, Z. Yu, Q. Yao, G. Rao, J. Wang, Highly Efficient Cool-White Photoluminescence of (Gua)₃Cu₂I₅ Single Crystals: Formation and Optical Properties, ACS Appl. Mater. Interfaces 13 (11) (2021) 13443-13451, 10.1021/acsami.1c02503
- [26] K.P. Bigalke, A. Hans, H. Hartl, Synthese und Strukturuntersuchungen von Iodocupraten(I). IX. Synthese und Kristallstrukturen von Cs₃Cu₂I₅ und RbCu₂I₃, Z. Anorg. Allg. Chem. 563 (1) (1988) 96-104, https://doi.org/10.1002/zaac.19885630114
- [27] C. Brink, C.H. MacGillavry, The crystal structure of K₂CuCl₃ and isomorphous substances, Acta Crystallographica 2 (3) (1949) 158-163, https://doi.org/10.1107/S0365110X49000436
- [28] S. Jagner, G. Helgesson, On the Coordination Number of the Metal in Crystalline Halogenocuprates(I) and Halogenoargentates(I), in: A.G. Sykes (Ed.), Adv. Inorg. Chem., Academic Press1991, pp. 1-45, https://doi.org/10.1016/S0898-8838(08)60004-5
- [29] Y. Hui, S. Chen, R. Lin, W. Zheng, F. Huang, Photophysics in $Cs_3Cu_2I_5$ and $CsCu_2I_3$, Mater. Chem. Front. 5 (19) (2021) 7088-7107, 10.1039/d1qm00552a
- [30] S. Andersson, S. Jagner, Crystal-Structures of Tetraphenylarsonium Dichlorocuprate(I), Tetraphenylphosphonium Dichlorocuprate(I) and Tetraphenylphosphonium Dibromocuprate(I), Acta Chem Scand A 39 (5) (1985) 297-305, DOI 10.3891/acta.chem.scand.39a-0297
- [31] G. Helgesson, S. Jagner, Two compounds containing dinuclear three-co-ordinated halogenoargentate(I) anions: crystal structures of bis(tetraphenylphosphonium) di-µ-chlorodichlorodiargentate(I) and bis(tetraphenylphosphonium) di-µ-bromodibromodiargentate(I), J. Chem. Soc., Dalton Trans. (8) (1988) 2117-2120, 10.1039/dt9880002117
- [32] L.-J. Xu, C.-Z. Sun, H. Xiao, Y. Wu, Z.-N. Chen, Green-Light-Emitting Diodes based on Tetrabromide Manganese(II) Complex through Solution Process, Adv. Mater. 29 (10) (2017) 1605739, https://doi.org/10.1002/adma.201605739
- [33] C. Zhou, M. Worku, J. Neu, H. Lin, Y. Tian, S. Lee, Y. Zhou, D. Han, S. Chen, A. Hao, P.I. Djurovich, T. Siegrist, M.-H. Du, B. Ma, Facile Preparation of Light Emitting Organic Metal

- Halide Crystals with Near-Unity Quantum Efficiency, Chem. Mater. 30 (7) (2018) 2374-2378, 10.1021/acs.chemmater.8b00129
- [34] J.P. Perdew, K. Burke, M. Ernzerhof, Generalized Gradient Approximation Made Simple, Phys. Rev. Lett. 77 (18) (1996) 3865-3868, 10.1103/PhysRevLett.77.3865
- [35] D.J.N. Singh, L., Planewaves, Pseudopotentials and the LAPW Method, 2nd ed., Springer, US, 2006, https://doi.org/10.1007/978-0-387-29684-5
- [36] P. Blaha, K. Schwarz, F. Tran, R. Laskowski, G.K.H. Madsen, L.D. Marks, WIEN2k: An APW+lo Program for Calculating the Properties of Solids, J. Chem. Phys. 152 (7) (2020) 074101, 10.1063/1.5143061
- [37] E. Sjöstedt, L. Nordström, D.J. Singh, An Alternative Way of Linearizing the Augmented Plane-Wave Method, Solid State Comm. 114 (1) (2000) 15-20, https://doi.org/10.1016/S0038-1098(99)00577-3
- [38] S. Alvarez, A Cartography of the Van der Waals Territories, Dalton Trans. 42 (24) (2013) 8617-8636, 10.1039/C3DT50599E
- [39] C. Janiak, A Critical Account on π – π Stacking in Metal Complexes with Aromatic Nitrogen-Containing Ligands, J. Chem. Soc., Dalton Trans. (21) (2000) 3885-3896, 10.1039/B003010O
- [40] L. Pauling, The Principles Determining the Structure of Complex Ionic Crystals, J. Am. Chem. Soc. 51 (4) (1929) 1010-1026, 10.1021/ja01379a006
- [41] C.Y. Yue, N. Lin, L. Gao, Y.X. Jin, Z.Y. Liu, Y.Y. Cao, S.S. Han, X.K. Lian, B. Hu, X.W. Lei, Organic cation directed one-dimensional cuprous halide compounds: syntheses, crystal structures and photoluminescence properties, Dalton Trans 48 (27) (2019) 10151-10159, 10.1039/c9dt01460h
- [42] L.J. Xu, A. Plaviak, X. Lin, M. Worku, Q. He, M. Chaaban, B.J. Kim, B. Ma, Metal Halide Regulated Photophysical Tuning of Zero-Dimensional Organic Metal Halide Hybrids: From Efficient Phosphorescence to Ultralong Afterglow, Angew. Chem. Int. Ed. 59 (51) (2020) 23067-23071, 10.1002/anie.202010555
- [43] T. Xu, Y. Li, M. Nikl, R. Kucerkova, Z. Zhou, J. Chen, Y.Y. Sun, G. Niu, J. Tang, Q. Wang, G. Ren, Y. Wu, Lead-Free Zero-Dimensional Organic-Copper(I) Halides as Stable and Sensitive X-ray Scintillators, ACS Appl. Mater. Interfaces. 14 (12) (2022) 14157-14164, 10.1021/acsami.1c23839
- [44] F. Liu, D. Mondal, K. Zhang, Y. Zhang, K. Huang, D. Wang, W. Yang, P. Mahadevan, R. Xie, Zero-dimensional Plate-shaped Copper Halide Crystals with Green-yellow Emissions, Mater. Adv. 2 (11) (2021) 3744-3751, 10.1039/d1ma00061f
- [45] H. Peng, B. Zou, Effects of Electron-Phonon Coupling and Spin-Spin Coupling on the Photoluminescence of Low-Dimensional Metal Halides, J. Phys. Chem. Lett. 13 (7) (2022) 1752-1764, 10.1021/acs.jpclett.1c03849

- [46] Y. Qiu, Z. Ma, Z. Li, H. Sun, G. Dai, X. Fu, H. Jiang, Z. Ma, Solely 3-Coordinated Organic-Inorganic Hybrid Copper(I) Halide: Hexagonal Channel Structure, Turn-On Response to Mechanical Force, Moisture, and Amine, Inorg. Chem. 61 (21) (2022) 8320-8327, 10.1021/acs.inorgchem.2c00781
- [47] H. Peng, X. Wang, Y. Tian, T. Dong, Y. Xiao, T. Huang, Y. Guo, J. Wang, B. Zou, Water-Stable Zero-Dimensional (C₄H₉)₄NCuCl₂ Single Crystal with Highly Efficient Broadband Green Emission, J Phys Chem Lett 12 (28) (2021) 6639-6647, 10.1021/acs.jpclett.1c01794
- [48] G.L. Chen, S.D. Guo, H. Feng, Z.S. Qian, Anion-regulated transient and persistent phosphorescence and size-dependent ultralong afterglow of organic ionic crystals, J Mater Chem C 7 (46) (2019) 14535-14542, 10.1039/c9tc04951g
- [49] M. Kasha, Characterization of electronic transitions in complex molecules, Discussions of the Faraday Society 9 (0) (1950) 14-19, 10.1039/DF9500900014
- [50] M. Vitale, W.E. Palke, P.C. Ford, Origins of the double emission of the tetranuclear copper(I) cluster Cu₄I₄(pyridine)₄: an ab initio study, J. Phys. Chem. 96 (21) (1992) 8329-8336, 10.1021/j100200a023
- [51] Y. Fang, W. Liu, S.J. Teat, G. Dey, Z. Shen, L. An, D. Yu, L. Wang, D.M. O'Carroll, J. Li, A Systematic Approach to Achieving High Performance Hybrid Lighting Phosphors with Excellent Thermaland Photostability, Adv. Funct. Mater. 27 (3) (2017) 1603444, https://doi.org/10.1002/adfm.201603444
- [52] S. Cheng, M. Nikl, A. Beitlerova, R. Kucerkova, X. Du, G. Niu, Y. Jia, J. Tang, G. Ren, Y. Wu, Ultrabright and Highly Efficient All-Inorganic Zero-Dimensional Perovskite Scintillators, Adv. Opt. Mater. 9 (13) (2021) 2100460, https://doi.org/10.1002/adom.202100460
- [53] Y. Chang, C.H. Grein, C.R. Becker, X.J. Wang, S. Sivananthan, Reduction of leakage currents in CdZnTe-based x-ray and gamma-ray detectors: a II-VI semiconductor superlattice approach, Proc.SPIE, 2010, p. 78050A.
- [54] E. Kamieniecki, Effect of charge trapping on effective carrier lifetime in compound semiconductors: High resistivity CdZnTe, J. Appl. Phys. 116 (19) (2014) 193702, 10.1063/1.4901826
- [55] J.N. Fru, N. Nombona, M. Diale, Characterization of sequential physical vapor deposited methylammonium lead tri-iodide perovskite thin films, Vacuum 182 (2020) 109727, https://doi.org/10.1016/j.vacuum.2020.109727
- [56] A. Kalam, R. Runjhun, A. Mahapatra, M.M. Tavakoli, S. Trivedi, H. Tavakoli Dastjerdi, P. Kumar, J. Lewiński, M. Pandey, D. Prochowicz, P. Yadav, Interpretation of Resistance, Capacitance, Defect Density, and Activation Energy Levels in Single-Crystalline MAPbI₃, J. Phys. Chem. C 124 (6) (2020) 3496-3502, 10.1021/acs.jpcc.9b11343

- [57] Y. Zhang, Y. Liu, Z. Xu, H. Ye, Z. Yang, J. You, M. Liu, Y. He, M.G. Kanatzidis, S. Liu, Nucleation-controlled Growth of Superior Lead-free Perovskite Cs₃Bi₂I₉ Single-crystals for High-performance X-ray Detection, Nat. Commun. 11 (1) (2020) 2304, 10.1038/s41467-020-16034-w
- [58] Z. Zhang, Y.-Z. Ma, L. Thomas, K. Gofryk, B. Saparov, Physical Properties of Candidate X-ray Detector Material Rb₄Ag₂BiBr₉, Cryst. Growth Des. 22 (2) (2022) 1066-1072, 10.1021/acs.cgd.1c00986
- [59] X. Geng, Q. Feng, R. Zhao, T. Hirtz, G. Dun, Z. Yan, J. Ren, H. Zhang, R. Liang, H. Tian, D. Xie, Y. Yang, T.L. Ren, High-Quality Single Crystal Perovskite for Highly Sensitive X-Ray Detector, IEEE Electron Device Letters 41 (2) (2020) 256-259, 10.1109/LED.2019.2960384
- [60] W. Pan, H. Wu, J. Luo, Z. Deng, C. Ge, C. Chen, X. Jiang, W.-J. Yin, G. Niu, L. Zhu, L. Yin, Y. Zhou, Q. Xie, X. Ke, M. Sui, J. Tang, Cs₂AgBiBr₆ single-crystal X-ray detectors with a low detection limit, Nature Photonics 11 (11) (2017) 726-732, 10.1038/s41566-017-0012-4
- [61] L. Lian, X. Wang, P. Zhang, J. Zhu, X. Zhang, J. Gao, S. Wang, G. Liang, D. Zhang, L. Gao, H. Song, R. Chen, X. Lan, W. Liang, G. Niu, J. Tang, J. Zhang, Highly Luminescent Zero-Dimensional Organic Copper Halides for X-ray Scintillation, J. Phys. Chem. Lett. 12 (29) (2021) 6919-6926, 10.1021/acs.jpclett.1c01946

TOC

 $(Ph_4P)MX_2$ (M=Cu, Ag; X=Cl, Br) exhibit zero-dimensional crystal structures featuring isolated linear $[CuX_2]^-$ and dimeric $[Ag_2Cl_4]^{2-}$ anions. The inclusion of the bulky organic cation Ph_4P^+ results in a much-improved air and thermal stability of these compounds. However, the electronic structures of $(Ph_4P)MX_2$ suggest optical transitions between spatially separated organic and inorganic motifs, leading to very weak onsets of optical absorption and unusually weak photoluminescence emission properties.

